

Silicon Donor Array as a Disordered One-Dimensional Electron Gas

Chao Lei¹ and Allan H. MacDonald¹

¹*Department of Physics, The University of Texas at Austin, Austin, Texas 78712, USA*

Donors in silicon can now be positioned with an accuracy of about one lattice constant, making it possible to form donor arrays for quantum computation or quantum simulation applications. However the multi-valley character of the silicon conduction band combines with central cell corrections to the donor state translate atomic scale imperfections in donor placement into strongly disordered inter-donor hybridization. We present a simple model that is able to account for central-cell corrections accurately, and use it to assess the impact of donor positional disorder on donor array properties in both itinerant and localized limits.

Introduction— One strategy for establishing robust solid-state quantum information processing hardware is to exploit the relatively simple bound states that surround donors or acceptors in the best understood semiconductor material, silicon [1, 2]. Considerable experimental progress has been made toward the use the electron spin of a donor-bound state in silicon, or alternately the donor nuclear spin, as a qubit [3–18]. It has been possible, for example, to achieve long coherence times for both electron [19, 20] and nuclear spins[21]. Additionally, advances in the technology for deterministically implanting donors in silicon [22–26] with high positional accuracy have made it possible to form donor arrays, which are attractive for both quantum computation [27] and quantum simulation [22, 28, 29] applications.

The physics of donor arrays in silicon is complicated by the presence of six valleys in the silicon conduction band, which adds an unwanted valley degree-of-freedom to donor-bound electron envelope function Hamiltonians. The valley degeneracy is fortunately lifted by central-cell corrections that couple valleys [30, 31]. There is still an unwanted complication, however, since mixing between valleys makes the interactions between donor levels extremely sensitive to donor positional disorder, as we will discuss in this paper. Even the lattice-constant-scale accuracy in donor positioning, now achievable in a silicon crystal [32], is not necessarily adequate. To describe this physics, we introduce a model for the central cell interactions that are responsible for valley splitting of donor levels in bulk silicon. The model is attractively simple and captures all the essential multi-valley physics. We use it to assess the effectiveness of recently proposed strategies [33, 34] to mitigate the influence of positional disorder on the exchange coupling between two spin qubits in the localized limit, and on donor array band properties in the itinerant limit.

Below we first present a calculation of valley-dependent tunneling in one-dimensional donor arrays, and then combine it with our simplified theory of valley-mixing by central cell corrections to quantify donor array disorder. In the localized limit, only donor spin degrees of freedom are relevant. We therefore use our model to calculate the exchange interactions between neighboring

spins, demonstrating that they are less sensitive to positional disorder when oriented along $\langle 110 \rangle$ rather than along $\langle 100 \rangle$, as demonstrated recently [33 and 34]. In the itinerant limit, positional disorder localizes donor array Bloch states. We show that this effect is also strongly limited by placing the donor array along $\langle 110 \rangle$. Our calculations demonstrate that central-cell corrections which separate the A_1 bound state from other disorder levels play a central role in determining donor-array properties in both localized and itinerant limits.

Donor array model— Donors in silicon have been well understood for decades [35–40]. Here we employ an effective-mass approach [35, 36] in which the wavefunction of an electron bound to an isolated donor has the form:

$$\psi(\mathbf{r}) = \sum_{\mu=1}^{N_{\mu}} F_{\mu}(\mathbf{r}) \phi_{\mu}(\mathbf{r}) \quad (1)$$

where μ labels valley, $N_{\mu} = 6$ is the number of valleys, $F_{\mu}(\mathbf{r})$ is an envelope function and $\phi_{\mu}(\mathbf{r}) = e^{i\mathbf{k}\cdot\mathbf{r}} u_{\mu}(\mathbf{r})$ is a band minimum Bloch function with periodic factor $u_{\mu}(\mathbf{r})$. When central cell corrections are neglected there is no coupling between valleys and donor-bound states in each valley are eigenstates of an effective mass Schrödinger equation[36] with Hamiltonian:

$$H = \sum_i \frac{\hbar^2}{2m_i^*} \nabla_i^2 + V(\mathbf{r}). \quad (2)$$

Here $i = x, y, z$, m_i are effective masses, and $V(\mathbf{r}) = -e^2/\epsilon|\mathbf{r}|^2$ is the hydrogenic external potential induced by the replacement of a Si atom by a donor ion at the origin. The mass tensor in Eq. 2 is diagonal because the six conduction band valleys in silicon are located along the principle cubic axes, with a large mass m_i for momentum along the valley direction (longitudinal mass $m_l \approx 0.98 m_0$ where m_0 is the bare electron mass) and a small mass for perpendicular momentum (transverse mass $m_t \approx 0.19 m_0$).

Because we are interested in a periodic array of donors, we use a plane-wave expansion approach and place donors at the center of three-dimensional supercells with

dimension $L_x \times L_y \times L_z$. The donor array envelope functions then depend on wavevector \mathbf{k} in the array mini-zone and can be expanded in the form:

$$|F_\mu(\mathbf{k})\rangle = \sum_{\mathbf{G}} C_{\mathbf{G}}(\mathbf{k}) |\mathbf{k} + \mathbf{G}\rangle, \quad (3)$$

where \mathbf{k} is the wavevector and \mathbf{G} is the supercell reciprocal lattice vectors (see [46] for more details). The kinetic energy is dependent on the spatial orientation of the donor array relative to the cubic axes. We limit our attention to donor arrays that have their \hat{z} -axis aligned with the silicon \hat{z} direction, but allow for changes of orientation θ of the donor array \hat{x} and \hat{y} directions relative to the silicon crystal \hat{x} and \hat{y} axes. For this family of donor array orientations

$$T_{\mu\mu'}^{\mathbf{G}\mathbf{G}'} = \delta_{\mu\mu'}^{\mathbf{G}\mathbf{G}'} \sum_i \frac{\hbar^2}{2m_i^*} \left(\sum_j (k_j + G_j) R_{ij}(\theta) \right)^2, \quad (4)$$

where $\delta_{\mu\mu'}^{\mathbf{G}\mathbf{G}'} \equiv \delta_{\mu\mu'} \delta_{\mathbf{G}\mathbf{G}'}$ and $R_{ij}(\theta)$ is the rotation matrix. The external potential of the donor array[41] is that produced by unit positive charges at the center of each supercell so that

$$V_{\mu,\mu'}^{\mathbf{G}\mathbf{G}'}(\mathbf{k}) = -\frac{1}{\Omega} \delta_{\mu\mu'} \frac{4\pi e^2}{\epsilon |\mathbf{G} - \mathbf{G}'|^2}, \quad (5)$$

where Ω is the supercell volume and $\epsilon \approx 11.7$ is the static dielectric constant of silicon.

As we show explicitly in Fig. S1 of the supplemental material [46], when all dimensions of the supercell approach infinity, the envelope functions approach hydrogenic wavefunctions and the donor binding energies approach $Ry = R_H m^* / \epsilon^2$ where $R_H \approx 13.6 \text{ eV}$ is the electron binding energy of hydrogen in vacuum, and $m^* \equiv (m_i^2 m_l)^{1/3}$ is the conduction band effective mass. In silicon $Ry \approx 32.6 \text{ meV}$ and the effective Bohr radius $a_B = a_0 \epsilon / m^* \approx 1.9 \text{ nm}$. In the one-dimensional case, the donor states form one-dimensional bands, the band dispersion is strongly valley-dependent as illustrated in Fig. 1, and sensitive to the spatial orientation of the donor array relative to the cubic axes for a given valley. Since the rotation of donor array happens in $\hat{x} - \hat{y}$ plane, hopping within $\pm z$ valleys mass is insensitive to the rotation angle θ , whereas for the $\pm x$ or $\pm y$ valleys, hopping on the array depends strongly on the the orientation angle. For a $\langle 110 \rangle$ orientation x -valley and y -valley hopping have identical amplitudes that are one order of magnitude smaller than for z -valley hopping.

Central cell corrections— So far we have neglected the central cell corrections that are important in silicon and yield donor-bound states that couple different valleys. The binding energies observed experimentally are 45.59 meV for the singly degenerate $1s(A_1)$ level [30, 42, 43], 32.58 meV for the doubly degenerate $1s(E)$ level, and 33.89 meV for the triply degenerate $1s(T_2)$ level. If we

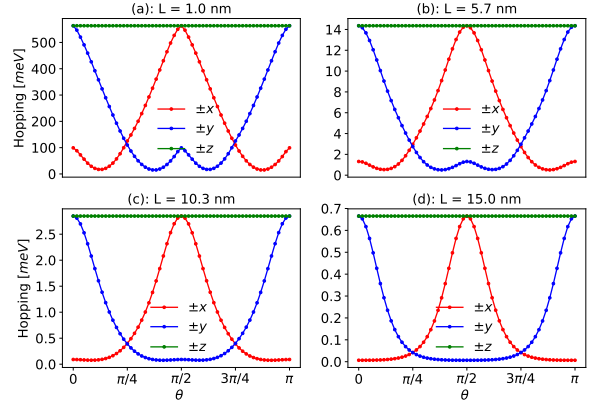


FIG. 1. Valley and orientation dependent near-neighbor hopping parameters for cubic donor-arrays with lattice constants L . The $\pm x$, $\pm y$ and $\pm z$ labels specify the Si conduction band valleys centered at $\mathbf{K}_\mu = \pm k_0 \hat{x}, \pm k_0 \hat{y}, \pm k_0 \hat{z}$, where $k_0 = 0.85\pi/a$ and a is the lattice constant of silicon.

ignore the small difference between the $1s(E)$ and $1s(T_2)$ levels, we can approximate the central cell correction to the single-particle Hamiltonian as the product of a single valley splitting energy scale $\epsilon_{vs} \approx 12 \text{ meV}$ [30, 44], an attractive delta-function $-\epsilon_{vs} \delta(\mathbf{r} - \mathbf{R})$ at the donor site \mathbf{R} , and a projection onto the donor states:

$$\mathcal{H}_{vs}(\mathbf{R}) = \frac{-\epsilon_{vs}}{N_\mu \Omega} \sum_{\substack{\mathbf{k}' \mathbf{k} \\ \mu' \mu}} |\mathbf{k}' \mu'\rangle \langle \mathbf{k} \mu| e^{i(\mathbf{K}_\mu + \mathbf{k} - \mathbf{K}_{\mu'} - \mathbf{k}') \cdot \mathbf{R}}, \quad (6)$$

where $\mathbf{K}_\mu = \pm k_0 \hat{x}, \pm k_0 \hat{y}, \pm k_0 \hat{z}$ are valley-momenta in bulk silicon, $k_0 = 0.85(2\pi/a)$, $a = 0.543 \text{ nm}$ is the conventional cubic lattice constant of bulk silicon, Because $\mathbf{K}_\mu - \mathbf{K}_{\mu'}$ is comparable in size to a reciprocal lattice vector, the valley splitting Hamiltonian changes substantially even for changes in \mathbf{R} that are on the atomic length scale. Note that Eq. 6 contains $\mu' \neq \mu$ terms that couple different valleys.

In order to calculate the parameters of a generalized Hubbard model for the donor array, we first Fourier transform the wavefunctions in the lowest energy band back to real space:

$$|\mathbf{R} \mu \sigma\rangle = \sum_{\mathbf{k}, \mathbf{G}} C_{\mathbf{k}\mathbf{G}}^{\mu\sigma} e^{-i\mathbf{k} \cdot \mathbf{R}} |\mathbf{k} + \mathbf{K}_\mu + \mathbf{G}\rangle |\sigma\rangle, \quad (7)$$

where μ labels valley, σ labels spin, \mathbf{R} is the position of the donor, and we have chosen $C_{\mathbf{k}\mathbf{G}=0}$ to be real and positive at each value of \mathbf{k} . The single-particle Hamiltonian in the Wannier representation defines the donor array hopping parameters $t_{\mathbf{R}\mathbf{R}'}^{\mu\mu'}$, which are a sum of kinetic energy ($T_{\mathbf{R}\mathbf{R}'}$) and external potential ($V_{\mathbf{R}\mathbf{R}'}^{\text{ext}}$) contributions (see [46] for more details).

In Fig. 2 (a) and (b) we plot hopping parameters for the $\pm x$ and $\pm y$ valleys as a function of donor separation and the spatial orientation of the donor array relative to

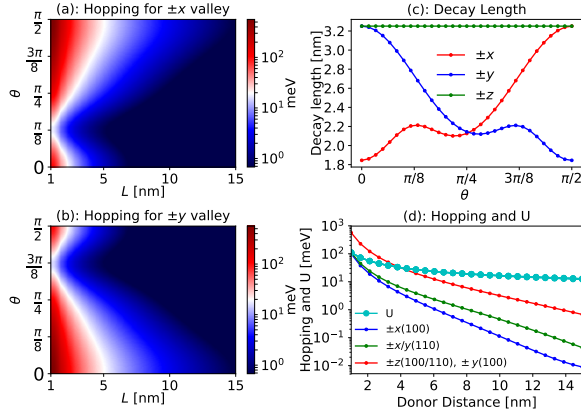


FIG. 2. Hopping parameters and on-site interactions of the silicon donor array Hubbard model *vs.* the donor separation and the spatial orientation of the donor array relative to the crystal x axis. The color scale plots in (a) and (b) show the hopping parameter *vs.* donor separation L and spatial orientation θ . (c) Decay lengths *vs.* θ for valley $\pm x$, $\pm y$ and $\pm z$. (d) Hubbard U and hopping parameters for donor arrays along the $\langle 100 \rangle$ and $\langle 110 \rangle$ directions.

the x axis. We see here that at small donor distances minima of the hopping parameters appear at $\theta \approx \pi/8$ for $\pm x$ valleys and at $\theta \approx 3\pi/8$ for $\pm y$ valleys. While for the $\pm z$ valley, the hopping parameters are independent of θ and the decay lengths of the hopping parameters extracted from the valley wavefunctions are nearly independent of θ . In the $\langle 100 \rangle$ direction both $\pm y$ and $\pm z$ effective masses are transverse (m_t) and therefore have the same decay length, which is larger than the $\pm x$ valley decay length which has the longitudinal effective mass m_l . Similar results apply for $\pm x$ and $\pm z$ valley in the 010 direction. Along the $\langle 110 \rangle$ direction ($\theta = \pi/4$) the decay lengths of $\pm x$ and $\pm y$ valleys are identical since the wavefunctions have equal contributions from transverse and longitudinal mass components.

The on-site Hubbard U can be calculated using $U_{\mu\mu'} = \langle \mathbf{R}\mu\sigma, \mathbf{R}\mu'\sigma' | V_c | \mathbf{R}\mu\sigma, \mathbf{R}\mu'\sigma' \rangle$ where $|\mathbf{R}\mu\sigma\rangle$ is a Wannier function and $V_c = e^2/\epsilon r^2$. In Fig. 2(d) we compare hopping parameters for donor arrays along the $\langle 100 \rangle$ and $\langle 110 \rangle$ directions. At small donor separation, valleys with transverse mass have larger hopping parameters that are large compared with U . However on-site electron-electron interaction strengths exceed the hopping parameters at larger donor separations; the ratio reaches ~ 10 when the donor separation is around 12 nm.

Valley Interference in Exchange Interactions— Using the Hubbard model parameters discussed above, we now assess the influence of valley degeneracy and donor placement on the exchange interactions between neighboring sites of a donor array. To calculate the exchange interactions we study a two-site Hubbard model which includes hopping, valley splitting, and on-site electron-electron in-

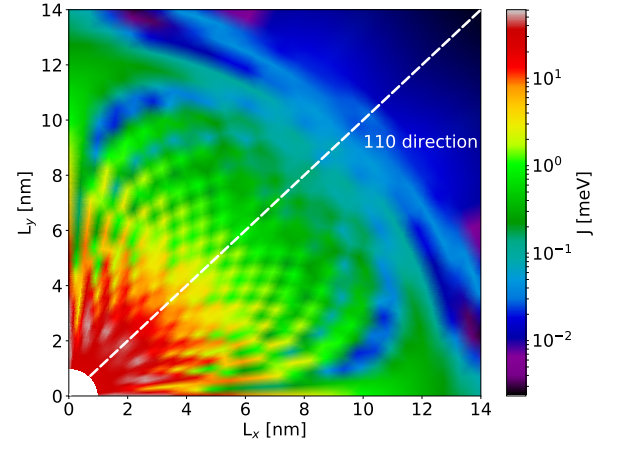


FIG. 3. Exchange interaction between two donors calculated with a two-site six-orbital Hubbard model. In explicit calculations, we place one of the two donors at the origin and the other at $\mathbf{L} = L(1, 0, 0)$, where L is the distance between two donors, and rotate the host-crystal cubic lattice by angle θ . The mapping from a $L - \theta$ grid to the plotted $L_x - L_y$ grid leads to some (white) regions in which there is no data. The white line labels the $\langle 110 \rangle$ direction.

teractions terms:

$$H = \sum_{\nu} t_{\mu} (c_{1\mu\sigma}^{\dagger} c_{2\mu\sigma} + h.c.) + \epsilon_{vs} \sum_{i,\mu\mu'} P_{\mu\mu'}^i c_{i\mu\sigma}^{\dagger} c_{i\mu'\sigma} + \sum_{i\mu\mu'\sigma\sigma'} U_{\mu\mu'} c_{i\mu\sigma}^{\dagger} c_{i\mu\sigma} c_{i\mu'\sigma'}^{\dagger} c_{i\mu'\sigma'} \quad (8)$$

Here t_{μ} is the inter-site hopping amplitude within valley \mathbf{K}_{μ} , $c_{i\mu\sigma}^{\dagger}$ ($c_{i\mu\sigma}$) is a creation (annihilation) operator, $P_{\mu\mu'}^i = e^{i(\mathbf{K}_{\mu} - \mathbf{K}_{\mu'}) \cdot \mathbf{R}}$ is the operator that applies a central-cell energy shift at site \mathbf{R} to the donor state, and $U_{\mu\mu'}$ is the on-site electron-electron interaction, which can be accurately modelled as valley independent. For one electron per donor, the charge excitation sector is gapped and low energy states are formed from spin degrees on each site. The exchange interaction between spins can therefore be defined in terms of the energy difference between the lowest energy two-electron singlet and triplet states: $J = E_T - E_S$.

In Fig. 3 we plot the exchange interaction *vs.* donor separation magnitude and direction. In our explicit calculations we place one of the two donors at the origin and the other at $\mathbf{L} = L(1, 0, 0)$, where L the distance between two donors, and rotate the host-crystal cubic lattice by angle θ . The $\pm z$ valleys always have a transverse effective mass m_t , which leads to large inter-site hopping amplitudes. Because the displacement \mathbf{L} is perpendicular to the $\pm z$ valley momenta \mathbf{K}_{μ} , the phase factors in the $(\pm z, \pm z)$ blocks of the valley-splitting Hamiltonian always vanish (i.e. $\hat{z} \cdot \mathbf{L} = 0$, with $\mathbf{L} \equiv \mathbf{R} - \mathbf{R}'$). For general θ both the $\pm x$ and $\pm y$ blocks of the valley splitting Hamiltonian at \mathbf{L} have non-trivial phase factors, which

change in value when L changes on an atomic length scale, and appear in the hopping amplitude between the two A_1 exciton levels. For $\theta = 0$ ($\theta = \pi/2$), $\pm x$ ($\pm y$)-valley hopping is longitudinal, and is therefore dominated by $\pm y$ ($\pm x$) and $\pm z$ valley components. It follows that the exchange energy is not sensitive to atomic scale position variations along the direction of the array, since both $\hat{y} \cdot \mathbf{L}$ ($\hat{x} \cdot \mathbf{L}$) and $\hat{z} \cdot \mathbf{L}$ are 0. However, there is a strong sensitivity to donor position variations in the direction perpendicular to donor array. In the $\langle 110 \rangle$ direction, the sensitivity of exchange interactions to donor placement is reduced in all in-plane directions since both $\pm x$ and $\pm y$ valley hopping strengths are reduced relative to $\pm z$ valley hopping. These results are consistent with recent experiments which have demonstrated a valley filtering effect on exchange interactions [33, 34], which is captured with a very simple model in this paper. As we explain in more detail in the next section, the lowest energy states become more concentrated in A_1 valley-split states at large donor separation, where ϵ_{vs} is larger than the hopping energies. The problem of exchange splitting has been considered previously [45] using the approximation, valid at large L , that the impurity-state Hamiltonian can be projected onto the A_1 basis, with qualitatively similar results for the large L limit.

Disorder and Localization— Donor placement in silicon often errs by a lattice constant or more. Even when a regular one-dimensional donor array is intended, the actual positions are $R_i = (n_i N_i + \delta_i) a \hat{r}_i$, where $\delta_i = 0, \pm 1$ randomly. Here $i = x, y, z$, $\hat{r}_i = \hat{x}, \hat{y}, \hat{z}$ are unit vectors along cubic axes, and N_i is the intended superlattice length in units of the silicon lattice constant a . As we see from Eq. 6, the random displacements introduce random phase factors $\exp i(\mathbf{K}_\mu - \mathbf{K}_{\mu'}) \cdot \mathbf{R}$ in the off-diagonal matrix elements of the valley-splitting Hamiltonian. (See [46] for further detail.) These phase factors account for changes in the positions at which the system gains energy by establishing constructive interference between valleys. The phase factors are sensitive to atomic scale placement inaccuracy because valley momenta are comparable in size to microscopic silicon primitive reciprocal lattice vectors, and much larger than the donor array superlattice primitive reciprocal lattice vectors. To study the influence of donor positional disorder on electronic properties we neglect interactions and calculate localization lengths using transfer matrices [47] for a model in which the $\exp(i\mathbf{K}_\mu \cdot \mathbf{R})$ ($\mu = x, y$) factors are modelled as independent random phase factors with phases Φ_μ . $\Phi_z = 0$ because the vertical component of the donor position is not expected to be disordered.

The Bloch state spectrum of donor arrays placed in $\langle 100 \rangle$ and $\langle 110 \rangle$ directions are shown in Fig. 4 (a). In the $L = 12$ nm case, illustrated in Fig. 4 (b), we see that the A_1 subband (lowered by ϵ_{vs}) is splitted out, and that the width of this subband corresponds to an effective hopping amplitude that is intermediate between the longitudinal

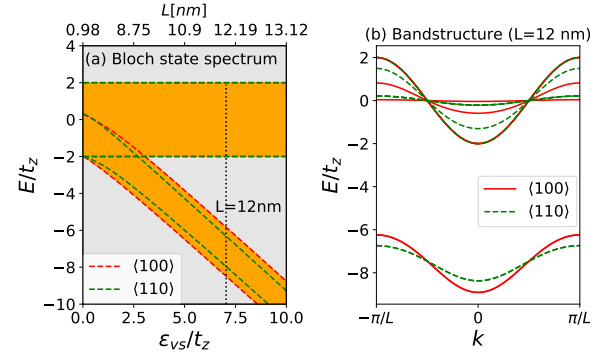


FIG. 4. (a) Bloch state spectrum *vs.* valley splitting strength $\epsilon_{vs} = 12\text{meV}$. Energies are in units of the hopping energy t_z . The corresponding donor separation L is indicated along the upper horizontal axis. The green and red dashed lines specify the band edges for donors placed along the $\langle 110 \rangle$ and $\langle 100 \rangle$ directions respectively and the orange regions are inside at least one of the six donor array bands for one of the two orientations. (b) quasi-1D bandstructures for $L = 12\text{nm}$ donor arrays along $\langle 100 \rangle$ and $\langle 110 \rangle$ directions respectively. The lowest energy (valley-split) A_1 band is singly degenerate in both cases. In the $\langle 100 \rangle$ ($\langle 110 \rangle$) case the top dispersive (middle flatter) band with width of $4t_z$ ($4t_{x/y}$) has degeneracy of 3.

and \hat{z} -direction values, which will be discussed further below.

The donor array orientation dependence of our results is most easily understood in the large ϵ_{vs} limit, where we can truncate the Hilbert space to the A_1 donor levels. The amplitude for hopping between A_1 levels is

$$t_{A1} = \frac{1}{6} \sum_{\mu} t_{\mu} \exp(i\Phi_{\mu}) \quad (9)$$

with $\Phi_z = 0$ and Φ_x and Φ_y imposed by random $\hat{x} - \hat{y}$ plane positional shifts of the two donors. Averaging over these phases we find that $\langle t_{A1} \rangle = t_z/3$ and the coefficient of variation (the square root of the variance divided by the mean) is

$$C_{A1}^v = \frac{\sigma_{A1}}{\langle t_{A1} \rangle} = \frac{\sqrt{t_x^2 + t_y^2}}{t_z}. \quad (10)$$

Here σ_{A1}^2 is the variance of t_{A1} and $\langle t_{A1} \rangle$ is its average value. The coefficient of variation for t_{A1} is dominated by the larger of t_x and t_y , and therefore reaches a minimum when $\theta = \pi/4$ since both t_x and t_y are reduced compared to t_z in this case. In Fig. 5 (a) we plot C_{A1}^v *vs.* θ for a series of L values. Here we see that the coefficient of variation of the hopping amplitude is close to 1 at $\theta = 0$, but reaches a minimum that drops with donor separation L at $\theta = \pi/4$. Hopping disorder is weaker for donor arrays aligned along $\langle 110 \rangle$ directions.

As a result of this reduced disorder, the localization lengths of the A_1 band electrons reaches a maximum at

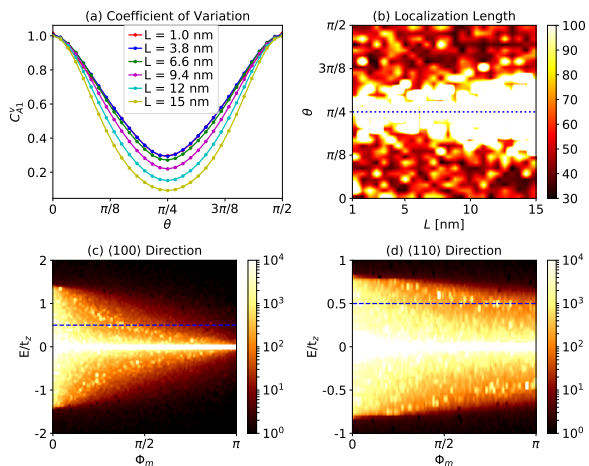


FIG. 5. (a) Coefficient of variation for hopping between A_1 states. Note that disorder is increasingly minimized at $\theta = \pi/4$ as L increases. (b) Localization in donor separation units *vs.* donor separation L and the orientation of the donor array relative to the x-axis θ at an energy $E = 0.5t_z$ above the middle of the disordered A_1 band. (c) and (d) illustrate the dependence of A_1 band localization length on disorder strength and energy for $L = 12$ nm. The dashed lines in (c) and (d) mark $E = 0.5t_z$, the energy used in (b).

$\theta = \pi/4$. The localization lengths are defined as the inverse of the smallest positive Lyapunov exponent averaged over phase disorder realizations: $\xi_{loc} = \langle \gamma_m \rangle_{avg}^{-1}$. (see supplemental material [46] for further detail). In Fig. 5 (b) we plot localization lengths calculated at an energy $0.5t_z$ from the center of the disordered A_1 band, with $\Phi_{x/y}$ sampled from the interval $(-\Phi_m, \Phi_m)$ and $\Phi_m = \pi/2$, we see that the localization lengths maximize at $\langle 110 \rangle$ direction. The A_1 band localization lengths are plotted *vs.* energy and Φ_m for $L = 12$ nm in Fig. 5 (c) and (d) for $\langle 100 \rangle$ and $\langle 110 \rangle$ directions respectively. for $\langle 110 \rangle$ -orientation donor arrays, localization lengths remain long near the center of the A_1 -band, even for strong donor-placement disorder.

Discussions — In summary, we have presented a theoretical model for a one-dimensional electron gas formed from donor arrays in silicon that accounts in a simple but accurate way for valley-dependent central-cell corrections to the donor energy. The model is based on the observations that there is an increase in donor binding energy ϵ_{vs} when all valley components of the donor wavefunction are in phase at the donor site. For donor separations less than ~ 4 nm, all six silicon valleys play an important role in low-energy many-electron states. At larger L , valley-splitting exceeds hopping energies and the low-energy physics can be approximated by a A_1 one-band model. Because the valley wavevectors are well separated in silicon, valley splitting leads to strong disorder in the hopping amplitude between the most strongly bound donor states, even when inaccuracy in donor placement

is only at the microscopic silicon lattice constant scale. It follows from our model that silicon donor arrays provide an excellent platform to study the combined influence of strong interactions and strong disorder in one-dimension.

The importance of interactions in silicon donor array states can be judged by evaluating the on-site Hubbard U . $U \sim 10$ meV exceeds the hopping parameters at larger donor separations, reaching a ratio of ~ 10 when the donor separation is around 12 nm. In this limit only spin-degrees of freedom are relevant, donor arrays are thus a platform to study the physics in one or two dimensional disordered many-body system, such as random field Heisenberg model [48] and one-dimensional Hubbard physics with hopping disorder [49–51]. In the limit of large L disorder can be weakened, but not eliminated, by orienting the donor array along the $\langle 110 \rangle$ -direction.

Acknowledgements— This work was supported by the Army Research Office (ARO) under contract W911NF-15-1-0561:P00001. We acknowledge the generous HPC resources provided by Texas Advanced Computing Center (TACC) at the University of Texas at Austin.

-
- [1] F. A. Zwanenburg, A. S. Dzurak, A. Morello, M. Y. Simmons, L. C. L. Hollenberg, G. Klimeck, S. Rogge, S. N. Coppersmith, and M. A. Eriksson, *Rev. Mod. Phys.* **85**, 961 (2013).
 - [2] P. L. Knight, E. A. Hinds, M. B. Plenio, R. G. Clark, R. Brenner, T. M. Buehler, V. Chan, N. J. Curson, A. S. Dzurak, E. Gauja, H. S. Goan, A. D. Greentree, T. Hallam, A. R. Hamilton, L. C. L. Hollenberg, D. N. Jamieson, J. C. McCallum, G. J. Milburn, J. L. O’Brien, L. Oberbeck, C. I. Pakes, S. D. Praver, D. J. Reilly, F. J. Ruess, S. R. Schofield, M. Y. Simmons, F. E. Stanley, R. P. Starrett, C. Wellard, and C. Yang, *Philosophical Transactions of the Royal Society of London. Series A: Mathematical, Physical and Engineering Sciences* **361**, 1451 (2003).
 - [3] J. J. Pla, K. Y. Tan, J. P. Dehollain, W. H. Lim, J. J. L. Morton, D. N. Jamieson, A. S. Dzurak, and A. Morello, *Nature* **489**, 541 (2012).
 - [4] H. Büch, S. Mahapatra, R. Rahman, A. Morello, and M. Y. Simmons, *Nat. Comm.* **4**, 2017 (2013).
 - [5] C. C. Lo, C. D. Weis, J. van Tol, J. Bokor, and T. Schenkel, *Phys. Rev. Lett.* **110**, 057601 (2013).
 - [6] J. J. Pla, F. A. Mohiyaddin, K. Y. Tan, J. P. Dehollain, R. Rahman, G. Klimeck, D. N. Jamieson, A. S. Dzurak, and A. Morello, *Phys. Rev. Lett.* **113**, 246801 (2014).
 - [7] R. Kalra, A. Laucht, C. D. Hill, and A. Morello, *Phys. Rev. X* **4**, 021044 (2014).
 - [8] A. J. Sigillito, A. M. Tyryshkin, T. Schenkel, A. A. Houck, and S. A. Lyon, *Nat. Nano.* **12**, 958 (2017).
 - [9] M. Veldhorst, C. H. Yang, J. C. C. Hwang, W. Huang, J. P. Dehollain, J. T. Muhonen, S. Simmons, A. Laucht, F. E. Hudson, K. M. Itoh, A. Morello, and A. S. Dzurak, *Nature* **526**, 410 (2015).
 - [10] Y. He, S. Gorman, D. Keith, L. Kranz, J. Keizer, and M. Simmons, *Nature* **571**, 371 (2019).

- [11] K. J. Morse, R. J. S. Abraham, A. DeAbreu, C. Bowness, T. S. Richards, H. Riemann, N. V. Abrosimov, P. Becker, H.-J. Pohl, M. L. W. Thewalt, and S. Simmons, *Science Advances* **3** (2017), 10.1126/sciadv.1700930.
- [12] S. J. Hile, L. Fricke, M. G. House, E. Peretz, C. Y. Chen, Y. Wang, M. Broome, S. K. Gorman, J. G. Keizer, R. Rahman, and M. Y. Simmons, *Science Advances* **4** (2018), 10.1126/sciadv.aag1459.
- [13] J. P. Dehollain, J. T. Muhonen, K. Y. Tan, A. Saraiva, D. N. Jamieson, A. S. Dzurak, and A. Morello, *Phys. Rev. Lett.* **112**, 236801 (2014).
- [14] M. A. Broome, T. F. Watson, D. Keith, S. K. Gorman, M. G. House, J. G. Keizer, S. J. Hile, W. Baker, and M. Y. Simmons, *Phys. Rev. Lett.* **119**, 046802 (2017).
- [15] D. M. Zajac, A. J. Sigillito, M. Russ, F. Borjans, J. M. Taylor, G. Burkard, and J. R. Petta, *Science* **359**, 439 (2018).
- [16] T. F. Watson, S. G. J. Philips, E. Kawakami, D. R. Ward, P. Scarlino, M. Veldhorst, D. E. Savage, M. G. Lagally, M. Friesen, S. N. Coppersmith, and et al., *Nature* **555**, 633–637 (2018).
- [17] M. A. Broome, S. K. Gorman, M. G. House, S. J. Hile, J. G. Keizer, D. Keith, C. D. Hill, T. F. Watson, W. J. Baker, L. C. L. Hollenberg, and et al., *Nature Communications* **9** (2018), 10.1038/s41467-018-02982-x.
- [18] Y. Wang, A. Tankasala, L. C. L. Hollenberg, G. Klimeck, M. Y. Simmons, and R. Rahman, *npj Quantum Information* **2** (2016), 10.1038/npjqi.2016.8.
- [19] A. M. Tyryshkin, S. Tojo, J. J. L. Morton, H. Riemann, N. V. Abrosimov, P. Becker, H.-J. Pohl, T. Schenkel, M. L. W. Thewalt, K. M. Itoh, and S. A. Lyon, *Nat. Mater.* **11**, 143 (2011).
- [20] T. F. Watson, B. Weber, Y.-L. Hsueh, L. C. L. Hollenberg, R. Rahman, and M. Y. Simmons, *Science Advances* **3** (2017), 10.1126/sciadv.1602811.
- [21] J. T. Muhonen, J. P. Dehollain, A. Laucht, F. E. Hudson, R. Kalra, T. Sekiguchi, K. M. Itoh, D. N. Jamieson, J. C. McCallum, A. S. Dzurak, and A. Morello, *Nat. Nano.* **9**, 986 (2014).
- [22] E. Prati, M. Hori, F. Guagliardo, G. Ferrari, and T. Shinada, *Nat. Nano.* **7**, 443 (2012).
- [23] J. A. Miwa, P. Hofmann, M. Y. Simmons, and J. W. Wells, *Phys. Rev. Lett.* **110**, 136801 (2013).
- [24] S. Shamim, S. Mahapatra, G. Scappucci, W. M. Klesse, M. Y. Simmons, and A. Ghosh, *Phys. Rev. Lett.* **112**, 236602 (2014).
- [25] E. Prati, K. Kumagai, M. Hori, and T. Shinada, *Sci. Rep.* **6**, 19704 (2016).
- [26] S. P. Cooil, F. Mazzola, H. W. Klemm, G. Peschel, Y. R. Niu, A. A. Zakharov, M. Y. Simmons, T. Schmidt, D. A. Evans, J. A. Miwa, and J. W. Wells, *ACS Nano* **11**, 1683 (2017), pMID: 28182399.
- [27] B. E. Kane, *Nature* **393**, 133 (1998).
- [28] J. Salfi, J. A. Mol, R. Rahman, G. Klimeck, M. Y. Simmons, L. C. L. Hollenberg, and S. Rogge, *Nat. Comm.* **7**, 11342 (2016).
- [29] F. Ansaloni, A. Chatterjee, H. Bohuslavskiy, B. Bertrand, L. Hutin, M. Vinet, and F. Kuemmeth, *Nature Communications* **11** (2020), 10.1038/s41467-020-20280-3.
- [30] B. Pajot and B. Clerjaud, *Optical Absorption of Impurities and Defects in Semiconducting Crystals: Electronic Absorption of Deep Centres and Vibrational Spectra*, Vol. 169 (Springer Science & Business Media, 2012).
- [31] K. E. J. Goh, F. Bussolotti, C. S. Lau, D. Kotekar-Patil, Z. E. Ooi, and J. Y. Chee, *Advanced Quantum Technologies* **3**, 1900123 (2020).
- [32] S. R. Schofield, N. J. Curson, M. Y. Simmons, F. J. Rueß, T. Hallam, L. Oberbeck, and R. G. Clark, *Phys. Rev. Lett.* **91**, 136104 (2003).
- [33] J. Salfi, B. Voisin, A. Tankasala, J. Bocquel, M. Usman, M. Y. Simmons, L. C. L. Hollenberg, R. Rahman, and S. Rogge, *Phys. Rev. X* **8**, 031049 (2018).
- [34] B. Voisin, J. Bocquel, A. Tankasala, M. Usman, J. Salfi, R. Rahman, M. Simmons, L. Hollenberg, and S. Rogge, *Nature communications* **11**, 1 (2020).
- [35] W. Kohn and J. M. Luttinger, *Phys. Rev.* **98**, 915 (1955).
- [36] J. M. Luttinger and W. Kohn, *Phys. Rev.* **97**, 869 (1955).
- [37] C. Kittel and A. H. Mitchell, *Phys. Rev.* **96**, 1488 (1954).
- [38] A. Baldereschi and N. O. Lipari, *Phys. Rev. B* **8**, 2697 (1973).
- [39] K. Shindo and H. Nara, *J. Phys. Soc. Jpn.* **40**, 1640 (1976).
- [40] A. L. Saraiva, M. J. Calderón, R. B. Capaz, X. Hu, S. Das Sarma, and B. Koiller, *Phys. Rev. B* **84**, 155320 (2011).
- [41] G. Giuliani and G. Vignale, *Quantum theory of the electron liquid* (Cambridge University Press, 2005).
- [42] A. K. Ramdas and S. Rodriguez, *Reports on Progress in Physics* **44**, 1297 (1981).
- [43] A. J. Mayur, M. D. Sciacca, A. K. Ramdas, and S. Rodriguez, *Phys. Rev. B* **48**, 10893 (1993).
- [44] J. K. Gamble, N. T. Jacobson, E. Nielsen, A. D. Baczewski, J. E. Moussa, I. Montañó, and R. P. Muller, *Phys. Rev. B* **91**, 235318 (2015).
- [45] B. Koiller, X. Hu, and S. Das Sarma, *Phys. Rev. Lett.* **88**, 027903 (2001).
- [46] See Supplemental Material at [URL] for more information.
- [47] C. W. J. Beenakker, *Rev. Mod. Phys.* **69**, 731 (1997).
- [48] M. Žnidarič, T. c. v. Prosen, and P. Prelovšek, *Phys. Rev. B* **77**, 064426 (2008).
- [49] A. W. Sandvik, D. J. Scalapino, and P. Henelius, *Phys. Rev. B* **50**, 10474 (1994).
- [50] A. N. Bloch, R. B. Weisman, and C. M. Varma, *Phys. Rev. Lett.* **28**, 753 (1972).
- [51] T. Giamarchi and B. S. Shastry, *Phys. Rev. B* **51**, 10915 (1995).